



Natural convection of water-based nanofluid in a chamber with a solid body of periodic volumetric heat generation

Marina S. Astanina¹ · Ioan Pop^{2,3} · Mikhail A. Sheremet¹

Received: 2 July 2022 / Accepted: 18 October 2022 / Published online: 19 November 2022
 © Akadémiai Kiadó, Budapest, Hungary 2022

Abstract

A computational analysis of convective energy transport of water-based nanosuspension having variable thermal properties has been performed using finite difference method. The considered square cavity includes cold vertical walls and adiabatic horizontal boundaries. The local heater of periodic thermal production is placed on the lower border of the domain. The working fluid is water with copper oxide nanoparticles of low concentration. Control differential equations with initial and boundary conditions have been written using non-dimensional stream function, vorticity and temperature. The resulting nonlinear partial differential equations with associated boundary conditions are solved using the finite difference methodology on a uniform calculation mesh. The analyzed control parameters including volumetric heat generation frequency, initial fraction of nanoparticles, heater location and time have been studied. The physics of the problem is well-explored for the embedded material parameters through tables and graphs. The obtained data have shown that the volumetric thermal production frequency of the source and the initial concentration of nanoparticles have the greatest influence on the heat transfer performance. The energy source temperature can be reduced by up to 20% by varying the characteristics of the source and nanosuspension.

Keywords Convective heat transfer · Heating element · Water-based nanofluid · Square chamber · Finite difference methodology

List of symbols

c	Heat capacity ($\text{J kg}^{-1} \text{K}^{-1}$)	k	Thermal conductivity ($\text{W m}^{-1} \text{K}^{-1}$)
C	Nanoparticles volume fraction	K	Additional function
d_p	Diameter of nanoparticles	L	Length of the enclosure (m)
$D_B = \frac{k_B}{3\pi\mu_f(T)d_p} T$	Dimensional Brownian diffusion coefficient	l	Distance from the left wall of the chamber to the left wall of the heater (m)
$\bar{D}_T = C \left[\frac{\mu_f(T)}{\rho_f} \right] \left(\frac{0.26 \cdot k_f}{2k_f + k_p} \right)$	Dimensional thermophoretic diffusion coefficient	$Le = \alpha_f / \bar{D}_B(T_c)$	Lewis number
D_B, D_T	Additional functions	M	Additional function
f	Volumetric thermal production frequency (s^{-1})	$\frac{Nu}{Nu}$	Nusselt number (–)
g	Gravity acceleration (m s^{-2})	Nu	Mean Nusselt number (–)
		$Nt = \bar{D}_B(T_c, C_0) \cdot \Delta T / (\alpha_f \cdot T_c)$	Thermophoresis parameter
		p	Static pressure (Pa)
		$Pr_T = \frac{\mu_f(T)}{\rho_f \alpha_f}$	Prandtl number (–)
		Q	Volumetric heat flux (W m^{-3})
		$Ra = \frac{g \cdot (\rho\beta)_f \cdot \Delta T \cdot L^3}{\mu_f(T_c) \cdot \alpha_f}$	Rayleigh number (–)
		T	Temperature (K)
		T_c	Cold wall temperature (K)
		t	Time (s)
		$\bar{u}, \bar{v}, \bar{w}$	Velocity projections (m s^{-1})

✉ Ioan Pop
 popm.ioan@yahoo.co.uk

¹ Laboratory on Convective Heat and Mass Transfer, Tomsk State University, Tomsk, Russia 634050

² Department of Mathematics, Babes-Bolyai University, 400084 Cluj-Napoca, Romania

³ Academy of Romanian Scientists, 3 Ilfov Street, 050044 Bucharest, Romania

u, v, w	Non-dimensional velocity projections (–)
$\bar{x}, \bar{y}, \bar{z}$	Coordinates (m)
x, y, z	Non-dimensional coordinates (–)

Greek symbols

α	Thermal diffusivity ($\text{W m}^{-2} \text{K}^{-1}$)
β	Thermal expansion coefficient (K^{-1})
γ	Dimensionless volumetric heat generation oscillation frequency
ΔT	Temperature drop (K)
$\delta = l/L$	Dimensionless distance from the left wall of the chamber to the left wall of the heater
θ	Non-dimensional temperature (–)
ρ	Density (kg m^{-3})
τ	Dimensionless time (–)
φ	Normalized nanoparticles volume fraction
$\bar{\psi}_x, \bar{\psi}_y, \bar{\psi}_z$	Vector potential functions ($\text{m}^2 \text{s}^{-1}$)
ψ_x, ψ_y, ψ_z	Non-dimensional vector potential functions (–)
$\bar{\omega}_x, \bar{\omega}_y, \bar{\omega}_z$	Projections of vorticity vector (s^{-1})
$\omega_x, \omega_y, \omega_z$	Dimensionless projections of vorticity vector (–)

Subscripts

c	Cooled
f	Fluid
hs	Heat source
nf	Nanofluid
p	Nanoparticles

Introduction

Over the past several years, researchers have paid close attention to the development of enhanced heat transfer fluids. To fulfill the industrial and technical demands, a smart liquid with improved heat capability is desirable. Nanotechnology is a rapidly expanding field in this modern age of advancement, where things are becoming smaller in size and getting better in the terminology of appropriate features. An area of particular importance is the preparation of products at the atomic and molecular levels for specific industrial purposes. One of the main ingredients of nanotechnology is nanofluid, which is primarily utilized to handle heat transfer challenges

effectively. To fulfill the industrial and technical demands, a smart fluid with outstanding thermal capability is desirable. Choi [1] in 1955 published an innovative heat transfer fluid that is based on nanotechnology called as nanofluid. A nanofluid is a suspension created in a base fluid by the uniform dispersion of very tiny dimension particles. The use of nanoparticles significantly enhances the thermophysical characteristics of conventional heat transfer fluid, hence increasing its heat transfer coefficient. Due to the widespread recognition, nanofluids are now extensively employed in a variety of industries, including automotive, electronics, solar energy, biomedical, oil recovery, food stuff, aerodynamics, geothermal systems, crude oil extractions, groundwater pollution, thermal insulation, heat exchanger, storage of nuclear waste, bulging construction, agriculture, thermal power plants, nuclear reactions, technologically advanced procedures, cost-effective and efficient cooling system refrigerators (see Das et al. [2], Nield and Bejan [3], Shenoy et al. [4] and Merkin et al. [5]). A nanofluid is a suspension that includes a host fluid and the uniform dispersion of very tiny particles. These particles have sizes ranging between 1 and 100 nm, and the material of these particles may be polymers, metals, metal oxides or other materials. An application of nanoadditives essentially augments the thermal parameters of conventional energy transport media, hence increasing its heat transfer coefficient. Convective flows in nanofluids have extensive engineering applications in aerodynamics, geothermal systems, building thermal insulation, heat exchanger, microelectronics, cancer therapy and others. In all of these applications, the heat conductivity of nanosuspension has a strong impact on the efficiency of the energy transport phenomenon. For such reason, scientists have continuously scrutinized the advantages and disadvantages of the nanosuspensions application (see Shenoy et al. [4] and Merkin et al. [5]).

Numerical simulation is an accessible and effective method for studying the problems of convective energy and mass transport. Interest in such studies is caused by a wide range of applications of the results obtained, including the rocket science, instrumentation, micro- and radio electronics, heating of buildings, etc. One of the striking examples of the application of the results is the development of cooling systems for heat-generated sources of various types. In such systems, good results are shown by the use of nanofluids as working fluids due to the possibility of varying their thermophysical properties by nanoparticles. Thus, Miroshnichenko et al. [6] have analyzed free convective energy and mass transport of $\text{Al}_2\text{O}_3/\text{H}_2\text{O}$ nanosuspension in a tilted open chamber having local hot element. It has been assumed that the top boundary of the cavity is open, and the nanoliquid penetrates into the chamber through it. The analysis has been carried out employing the Oberbeck–Boussinesq equations written using dimensionless stream function, vorticity and

temperature. The influence of the cavity inclination angle, the heater position and the nanoparticles concentration has been demonstrated. It has been revealed that the optimal selection of the considered parameters makes it possible to minimize the average temperature of the heater. The most efficient cooling of the thermally producing blocks is observed when it is placed in the center of the cavity at an angle of inclination of the chamber equaled to $\pi/3$. A computational analysis of thermal convection of $\text{Al}_2\text{O}_3/\text{H}_2\text{O}$ nanofluid inside a closed chamber with a thick bottom wall heated unevenly (according to the sinusoidal law) has been carried out by Bouchoucha et al. [7]. The finite volume technique has been employed to work out the control equations. The outcomes have been shown as streamlines, isotherms, local and average Nu profiles for different values of the Rayleigh number, nanoadditives concentration and the thickness of the bottom wall. The outcomes obtained have shown a decrease in the mean Nu with an increase in the thickness of the bottom wall. Bondarenko et al. [8] have visualized the natural convective flow of $\text{Al}_2\text{O}_3/\text{H}_2\text{O}$ nanosuspension in a closed square chamber with a thermally producing block. Cooling of the cavity occurs from the vertical walls. The impact of the nanoadditives concentration and the location of the heater on transport phenomena in the cavity and heat removal from the heated element has been shown. The authors have revealed that an inclusion of nanoadditives can improve the cooling phenomenon when the energy source is close to the vertical cold surface. Mahmoodi [9] has presented results of mathematical modeling of natural convection of nanofluids ($\text{Ag}/\text{H}_2\text{O}$, $\text{Cu}/\text{H}_2\text{O}$, $\text{Ti}_2\text{O}/\text{H}_2\text{O}$) inside closed 2D chamber with a flat horizontal/vertical heater in the center of the cavity and cold vertical walls. The results have shown that $\text{Ag}/\text{H}_2\text{O}$ nanofluid has more effective properties for heat removing from the heater for high Ra. Low Rayleigh numbers have reflected low sensitivity to the type of nanofluids.

Keramat et al. [10] have numerically examined the free convection of alumina–water nanosuspension within closed H-shaped cavity with baffle at $10^4 < \text{Ra} < 10^6$. It has been demonstrated that a raise of Ra and nanoadditives volume fraction enhances the energy transport inside the cavity. Islam et al. [11] have conducted the computational analysis of CNT-water nanosuspension thermal convection within a triangular chamber under the sinusoidal heating influence from the bottom wall by employing the finite difference technique. The outcomes have shown that an increment in Ra results to a raise of the fluctuations amplitude in the average Nusselt number. Nabwey et al. [12] have presented results of numerical calculation of $\text{Cu}/\text{H}_2\text{O}$ nanofluid heat transfer within an inclined U-chamber in the presence of local energy element and magnetic field. The obtained data have illustrated that the location of the heating section and the value of the Hartmann number have the most essential impact

on the energy transport strength in the chamber. Alsabery et al. [13] have scrutinized the mixed convection of $\text{Al}_2\text{O}_3/\text{H}_2\text{O}$ nanosuspension inside 2D chamber with wavy vertical walls and isothermal heating from the bottom boundary or solid inner block. The obtained outcomes reflect significant changes in the flow structure with a raise of the nanoadditives concentration and the introduction of a solid element on the bottom wall compared to a flat isothermal boundary. Reviews on the researches of energy transport in various regions filled with nanofluids under different boundary conditions have been presented by Narankhishig et al. [14] and Sheikholeslami and Rokni [15]. The problems of convective heat transfer under the magnetic impact have been shown by Narankhishig et al. [14], while Sheikholeslami and Rokni [15] have presented the results of numerical simulation of nanosuspension heat and mass transport under the magnetic impact inside different cavities. Two models have been shown, namely MHD and FHD.

It should be noted that copper nanoparticles are among the most effective carriers among different nanoadditives owing to high heat conductivity of the copper. Selimefendigil et al. [16] have simulated the mixed convection in a square porous chamber filled with a $\text{CuO}/\text{H}_2\text{O}$ nanosuspension. The cavity contains a porous insert in the lower part and a rotating adiabatic cylinder in the central part of the body. The chamber is warmed from the lower border and cooled from the upper boundary. The impact of Ra, the angular velocity of rotation, the nanoadditives volume fraction, the Darcy number, and the position of the cylinder in the cavity on the performance of the thermal system has been shown. The authors have shown that energy transport strength increases with a growth of Ra, angular velocity of rotation of the cylinder and nanoadditives volume fraction, and Da. Vijaybabu [17] has demonstrated simulation data of the convective motion of $\text{CuO}/\text{H}_2\text{O}$ nanosuspension in a closed square chamber having isothermally heated round porous body. It has been found that the flow rate of a liquid increases with an increment in Da and nanoadditives volume fraction in the working liquid. Mathematical modeling of heat transfer of $\text{CuO}/\text{H}_2\text{O}$ nanosuspension in a porous chamber with open areas has been performed by Biswas et al. [18]. The porous medium has been modeled taking into account the Darcy–Brinkman–Forchheimer approach. The results have shown that the heat transfer rate of the host liquid is highly dependent on the governing parameters (Reynolds number, Darcy number, Richardson number, porosity, nanoparticles volume fraction and cavity geometry parameter). An assessment of the efficiency of heat removal by adding nanoparticles to the working medium has been performed. Sivasankaran et al. [19] have analyzed the thermal convection of $\text{CuO}/\text{H}_2\text{O}$ nanosuspension in a tilted chamber having thermally producing porous medium. In the simulation, a local heat non-equilibrium model has been employed. The

chamber is warmed from the horizontal bottom border and cooled from the vertical boundaries. The results obtained have shown that the energy transport strength decreases with a raise of the nanoadditives volume fraction for the case of high Rayleigh numbers. The intensification of energy transfer is achieved by increasing the values of the modified conductivity coefficient and the porosity of the material. A numerical study of the thermal convection of water-based nanoliquids with the addition of Cu, Al_2O_3 , TiO_2 nanoadditives in regions of various geometries with warmed and cooled cylinders has been carried out by Garoosi et al. [20]. The simulation results have shown that at low Ra, the energy transport strength decreases with a change in the shape of the body from square to triangular. It has been also found that for each Rayleigh number, an optimal nanoadditives concentration with high energy transport strength inside the chamber can be defined. Emami et al. [21] have examined the thermal convection of a water-based nanofluid with the addition of copper particles in a tilted porous chamber. The influence of chamber tilted angle, heater shape, properties of nanosuspension and porous medium on the energy transport characteristics has been examined. The results have shown that the choice of heater shape (side or corner heating) and angle of inclination at different nanofluid concentrations and different properties of the porous medium can greatly affect the heat transfer characteristics. Bouzerzour et al. [22] have demonstrated the results of free convection simulation within annulus filled with $\text{CuO}/\text{H}_2\text{O}$ nanofluids in the presence of local heaters. The results have shown the best heat removal at high Ra and the nanoadditives concentration.

In some cases, alumina particles are added to the base fluid along with copper oxide particles. Such combination can intensify the heat transport within the chamber. Thus, the thermogravitational energy transport of $\text{Cu}/\text{Al}_2\text{O}_3/\text{H}_2\text{O}$ hybrid nanosuspension in a partially open square chamber with a fixed isothermally heated vertical partition under the magnetic impact has been scrutinized by Du et al. [23]. The finite difference procedure has been used to work out the Navier–Stokes equations. The results have shown that an increment in the nanoadditives concentration in the liquid enhances the rate of heat transfer inside the cavity. Mixed convection within horizontal channel under the magnetic impact has been examined computationally by Nath and Murugesan [24]. The impact of the magnetic field tilted angle and the characteristics of the nanofluid on the hydrodynamics of the flow in the channel has been shown. Rana et al. [25] have demonstrated the outcomes of computational analysis of hybrid nanoliquid in closed cavity with inner bodies of different types by employing the Galerkin finite element algorithm. The authors have shown a strong dependence of the mean Nu on the volume concentration of nanoparticles. Valuable published papers on classical viscous fluids and nanofluids are also those by Roy [26–29],

Roy et al. [30], Parvin et al. [31], Saha et al. [32], Sajid and Ali [33], Sajid and Bicer [34, 35], Sajid et al. [36, 37], and Hawaz et al. [38].

It can be seen from the presented brief review that studies on heat transfer in areas filled with two-phase liquids have been started recently and require additional analysis. Motivated by the preceding work, the primary goal of this present research is to present a mathematical modeling of the thermogravitational energy transport of $\text{CuO}/\text{H}_2\text{O}$ nanosuspension in a closed square chamber with an energy source of periodic heat generation and cooling vertical walls. The thermophysical properties of the working liquid considered are dependent on temperature and the nanoadditives volume fraction. The obtained results are related to the modeling of passive cooling systems for heating elements and various thermal systems. $\text{CuO}/\text{H}_2\text{O}$ is chosen as the nanoparticle since it has been widely used in numerous studies. The initial nanoparticles concentration (C_0) have been considered in the range between 0.0 and 0.04. It should be noted that the use of CuO as nanoparticles is an effective way to intensify heat transfer due to the high thermal conductivity properties of copper oxide. Moreover, the considered temperature- and concentration-dependent relations for the thermal conductivity and dynamic viscosity have been verified by many authors for the considered nanoparticles material.

Mathematical model and basic assumptions

The schematic model of considered natural convection problem is shown in Fig. 1. The thermogravitational energy transport of a viscous nanofluid (a mixture of water and copper oxide nanoparticles) in a closed chamber having thermally producing solid block placed on the lower border is considered. The volumetric heat generation of the source is described by the following relation $Q(t) = 0.5Q_0\{1 - \cos(ft)\}$. The vertical borders of the chamber are assumed to be isothermally cooling, while the horizontal surfaces are considered to be adiabatic. The force

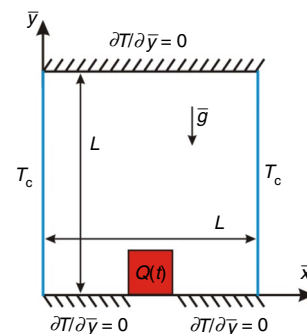


Fig. 1 Physical model

of gravity is directed vertically downward. The chamber is saturated with a Newtonian heat-conducting water-based nanosuspension. It is supposed that water and nanoadditives are in heat equilibrium, and only Brownian diffusion and thermal diffusion are considered as the main mechanisms of the relative motion of nanoparticles inside the carrier medium. The thermal properties of the nanoparticle material and water are given in Table 1. It is also assumed that the properties of a nanoliquid depend on temperature and the nanoadditives volume fraction.

The transport of mass, momentum and energy within the chamber is assumed to be 2D, laminar, with a negligible effect of viscous dissipation and the work of pressure forces. The Boussinesq approximation is used to describe the influence of the buoyancy force. Considering these conditions, the governing equations can be formulated as follows (see Astanina et al. [39, 40]):

$$\frac{\partial \bar{u}}{\partial \bar{x}} + \frac{\partial \bar{v}}{\partial \bar{y}} = 0 \tag{1}$$

$$\begin{aligned} \rho_{nf} \left(\frac{\partial \bar{u}}{\partial t} + \bar{u} \frac{\partial \bar{u}}{\partial \bar{x}} + \bar{v} \frac{\partial \bar{u}}{\partial \bar{y}} \right) &= - \frac{\partial p}{\partial \bar{x}} + 2 \frac{\partial}{\partial \bar{x}} \left(\bar{\mu}_{nf}(T, C) \frac{\partial \bar{u}}{\partial \bar{x}} \right) \\ &+ \frac{\partial}{\partial \bar{y}} \left[\bar{\mu}_{nf}(T, C) \left(\frac{\partial \bar{u}}{\partial \bar{y}} + \frac{\partial \bar{v}}{\partial \bar{x}} \right) \right] \end{aligned} \tag{2}$$

$$\begin{aligned} \rho_{nf} \left(\frac{\partial \bar{v}}{\partial t} + \bar{u} \frac{\partial \bar{v}}{\partial \bar{x}} + \bar{v} \frac{\partial \bar{v}}{\partial \bar{y}} \right) &= - \frac{\partial p}{\partial \bar{y}} + 2 \frac{\partial}{\partial \bar{y}} \left(\bar{\mu}_{nf}(T, C) \frac{\partial \bar{v}}{\partial \bar{y}} \right) \\ &+ \frac{\partial}{\partial \bar{x}} \left[\bar{\mu}_{nf}(T, C) \left(\frac{\partial \bar{u}}{\partial \bar{y}} + \frac{\partial \bar{v}}{\partial \bar{x}} \right) \right] \\ &+ (\rho\beta)_{nf} g (T - T_c) \end{aligned} \tag{3}$$

$$\begin{aligned} (\rho c)_{nf} \left(\frac{\partial T}{\partial t} + \bar{u} \frac{\partial T}{\partial \bar{x}} + \bar{v} \frac{\partial T}{\partial \bar{y}} \right) &= \frac{\partial}{\partial \bar{x}} \left(k_{nf} \frac{\partial T}{\partial \bar{x}} \right) + \frac{\partial}{\partial \bar{y}} \left(k_{nf} \frac{\partial T}{\partial \bar{y}} \right) \\ &+ (\rho c)_p \left\{ \bar{D}_B \left(\frac{\partial C}{\partial \bar{x}} \frac{\partial T}{\partial \bar{x}} + \frac{\partial C}{\partial \bar{y}} \frac{\partial T}{\partial \bar{y}} \right) \right. \\ &\left. + \frac{\bar{D}_T}{T_c} \left[\left(\frac{\partial T}{\partial \bar{x}} \right)^2 + \left(\frac{\partial T}{\partial \bar{y}} \right)^2 \right] \right\} \end{aligned} \tag{4}$$

$$\begin{aligned} \frac{\partial C}{\partial t} + \bar{u} \frac{\partial C}{\partial \bar{x}} + \bar{v} \frac{\partial C}{\partial \bar{y}} &= \frac{\partial}{\partial \bar{x}} \left(\bar{D}_B \frac{\partial C}{\partial \bar{x}} + \frac{\bar{D}_T}{T_c} \frac{\partial T}{\partial \bar{x}} \right) \\ &+ \frac{\partial}{\partial \bar{y}} \left(\bar{D}_B \frac{\partial C}{\partial \bar{y}} + \frac{\bar{D}_T}{T_c} \frac{\partial T}{\partial \bar{y}} \right) \end{aligned} \tag{5}$$

Table 1 Thermal properties of the working fluid and nanoadditives material

Thermophysical characteristics	H ₂ O	CuO
$\rho/\text{kg m}^{-3}$	997.1	6500
$c_p/\text{J kg}^{-1} \text{K}^{-1}$	4179	540
$k/\text{W m}^{-1} \text{K}^{-1}$	0.613	18
d_p/nm	0.384	29
$\alpha \times 10^{-7}/\text{m}^2 \text{c}^{-1}$	1.47	51.28
$\beta \times 10^{-5}/1 \text{K}^{-1}$	21	0.85

$$(\rho c)_{hs} \frac{\partial T}{\partial t} = k_{hs} \left(\frac{\partial^2 T}{\partial \bar{x}^2} + \frac{\partial^2 T}{\partial \bar{y}^2} \right) + Q(t) \tag{6}$$

The nanosuspension density, thermal capacity and heat parameter of volumetric expansion of a nanofluid are determined as follows:

$$\rho_{nf} = (1 - C)\rho_f + C\rho_p \tag{7}$$

$$(\rho c)_{nf} = (1 - C)(\rho c)_f + C(\rho c)_p \tag{8}$$

$$(\rho\beta)_{nf} = (1 - C)(\rho\beta)_f + C(\rho\beta)_p \tag{9}$$

The Brownian diffusion parameter \bar{D}_B can be determined on the basis of the Einstein–Stokes relation in the form $\bar{D}_B = \frac{k_B}{3\pi\mu_f(T)d_p} T$; to determine the thermal diffusion parameter \bar{D}_T , we can use the relation of the form $\bar{D}_T = C \left[\frac{\mu_f(T)}{\rho_f} \right] \left(\frac{0.26 \cdot k_f}{2k_f + k_p} \right)$. Here, $k_B = 1.3807 \times 10^{-23} \text{ J K}^{-1}$ is the Boltzmann parameter, d_p is the nanoadditives size.

The nanosuspension heat conductivity is determined based on the Chon model [41] in the form:

$$\frac{k_{nf}}{k_f} = 1 + 64.7 \cdot C^{0.764} \left(\frac{d_f}{d_p} \right)^{0.369} \left(\frac{k_f}{k_p} \right)^{0.7476} \text{Pr}_T^{0.9955} \text{Re}^{1.2321} \tag{10}$$

Here, $\text{Pr}_T = \frac{\mu_f(T)}{\rho_f \alpha_f}$ is the Prandtl number, $\text{Re} = \frac{\rho_f k_B}{3\pi[\mu_f(T)]^2 l_f} T$ is the Reynolds number, $l_f = 0.17 \text{ nm}$ is the mean free path of the host liquid molecule (see Chon et al. [41]). The presented relation (10) makes it possible to analyze the influence of the size of nanoparticles and temperature on the heat conductivity of a nanofluid in a wide range of temperatures at $1\% \leq C \leq 9\%$ (see Chon et al. [41] and Abu-Nada et al. [42]).

The nanosuspension viscosity is determined as follows (see Chon et al. [41], Abu-Nada et al. [42], Haddad et al. [43] and Nguyen et al. [44]):

$$\begin{aligned} \mu_{nf}(T, C) = & -0.6967 \times 10^{-3} + \frac{1.5937 \times 10^{-2}}{T - 273.15} + 1.238 \times 10^{-3} C \\ & + \frac{1.35614}{(T - 273.15)^2} - 0.259 \times 10^{-3} C^2 \\ & - 3.088 \times 10^{-2} \left(\frac{C}{T - 273.15} \right) - \frac{19.65274}{(T - 273.15)^3} \\ & + 0.01593 \times 10^{-3} C^3 + 4.38206 \times 10^{-3} \left(\frac{C^2}{T - 273.15} \right) \\ & + 0.147573 \frac{C}{(T - 273.15)^2} \end{aligned} \tag{11}$$

The dynamic viscosity of water is (see Chon et al. [41] and Nguyen et al. [44]):

$$\mu_f(T) = 2.414 \times 10^{-5} \times 10^{247.8/(T-140)} \tag{12}$$

The formulated dimensional partial differential Eqs. (1) to (6) can be dimensionalized using the following relations:

$$\begin{aligned} x = \bar{x}/L, \quad y = \bar{y}/L, \quad \tau = t\sqrt{g\beta_f\Delta T/L}, \quad u = \bar{u}/\sqrt{g\beta_f\Delta TL}, \\ v = \bar{v}/\sqrt{g\beta_f\Delta TL}, \quad \theta = (T - T_c)/\Delta T, \quad \phi = C/C_0, \quad M = \mu_{nf}(T, C)/\mu_f(T_c), \\ K = k_{nf}(T, C)/k_f, \quad D_B = \bar{D}_B(T)/\bar{D}_B(T_c), \quad D_T = \bar{D}_T(T, C)/\bar{D}_T(T_c, C_0) \end{aligned} \tag{13}$$

Also with the use of new dimensionless stream function ψ ($u = \frac{\partial\psi}{\partial y}$, $v = -\frac{\partial\psi}{\partial x}$) and vorticity $\omega = \frac{\partial v}{\partial x} - \frac{\partial u}{\partial y}$, therefore, the non-dimensional control equations are

$$\frac{\partial^2\psi}{\partial x^2} + \frac{\partial^2\psi}{\partial y^2} = -\omega \tag{14}$$

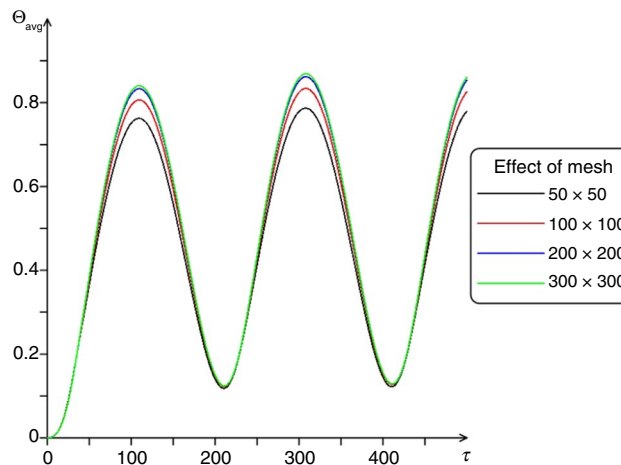


Fig. 2 Influence of grid parameters on average heater temperature at $Ra = 10^6$, $Pr = 6.52$, $Le = 9415.6$, $Nt = 2.56^{-7}$, $C_0 = 0.04$, $\gamma = 0.01$, $\delta = 0.4$

$$\begin{aligned} \frac{\partial\phi}{\partial\tau} + u \frac{\partial\phi}{\partial x} + v \frac{\partial\phi}{\partial y} = & \frac{1}{Le\sqrt{Ra} \cdot Pr} \left[\frac{\partial}{\partial x} \left(D_B \frac{\partial\phi}{\partial x} \right) + \frac{\partial}{\partial y} \left(D_B \frac{\partial\phi}{\partial y} \right) \right] \\ & + \frac{Nt}{C_0\sqrt{Ra} \cdot Pr} \left[\frac{\partial}{\partial x} \left(D_T \frac{\partial\theta}{\partial x} \right) + \frac{\partial}{\partial y} \left(D_T \frac{\partial\theta}{\partial y} \right) \right] \end{aligned} \tag{17}$$

$$\begin{aligned} \frac{\partial\omega}{\partial\tau} + u \frac{\partial\omega}{\partial x} + v \frac{\partial\omega}{\partial y} = & \frac{1}{1 - \phi C_0 + \phi C_0 \cdot \rho_p/\rho_f} \sqrt{\frac{Pr}{Ra}} \left[\frac{\partial^2(M\omega)}{\partial x^2} + \frac{\partial^2(M\omega)}{\partial y^2} \right] \\ & + \frac{1 - \phi C_0 + \phi C_0 \cdot (\rho\beta)_p/(\rho\beta)_f}{1 - \phi C_0 + \phi C_0 \cdot \rho_p/\rho_f} \frac{\partial\theta}{\partial x} + \frac{2}{1 - \phi C_0 + \phi C_0 \cdot \rho_p/\rho_f} \sqrt{\frac{Pr}{Ra}} \\ & \times \left[\frac{\partial^2 M}{\partial x^2} \frac{\partial u}{\partial y} - \frac{\partial^2 M}{\partial y^2} \frac{\partial v}{\partial x} + \frac{\partial^2 M}{\partial x \partial y} \left(\frac{\partial v}{\partial y} - \frac{\partial u}{\partial x} \right) \right] \end{aligned} \tag{15}$$

$$\begin{aligned} \frac{\partial\theta}{\partial\tau} + u \frac{\partial\theta}{\partial x} + v \frac{\partial\theta}{\partial y} = & \frac{1}{\left[1 - \phi C_0 + \phi C_0 \cdot (\rho c_p)_p/(\rho c_p)_f \right] \sqrt{Ra} \cdot Pr} \left[\frac{\partial}{\partial x} \left(K \frac{\partial\theta}{\partial x} \right) + \frac{\partial}{\partial y} \left(K \frac{\partial\theta}{\partial y} \right) \right] \\ & + \frac{D_B \cdot C_0}{\left[\phi C_0 + (1 - \phi C_0) \cdot (\rho c_p)_f/(\rho c_p)_p \right] Le\sqrt{Ra} \cdot Pr} \left(\frac{\partial\phi}{\partial x} \frac{\partial\theta}{\partial x} + \frac{\partial\phi}{\partial y} \frac{\partial\theta}{\partial y} \right) \\ & + \frac{D_T \cdot Nt}{\left[\phi C_0 + (1 - \phi C_0) \cdot (\rho c_p)_f/(\rho c_p)_p \right] \sqrt{Ra} \cdot Pr} \left[\left(\frac{\partial\theta}{\partial x} \right)^2 + \left(\frac{\partial\theta}{\partial y} \right)^2 \right] \end{aligned} \tag{16}$$

$$\frac{\partial \theta}{\partial \tau} = \frac{\alpha_{hs}/\alpha_f}{\sqrt{Pr \cdot Ra}} \left(\frac{\partial^2 \theta}{\partial x^2} + \frac{\partial^2 \theta}{\partial y^2} + \frac{k_f}{2k_{hs}} \{1 - \cos(\gamma \tau)\} \right) \quad (18) \quad D_T = \frac{C \cdot \mu_f(T)}{C_0 \cdot \mu_f(T_c)} = \phi \cdot 10^{\frac{247.8 \cdot \theta \Delta T}{(\theta \Delta T + T_c - 140)(140 - T_c)}}$$

The formulated equations are affected with conditions:

$$\begin{aligned} \tau = 0: \quad & \psi = \omega = \theta = 0, \quad \phi = 1; \\ \tau > 0: \quad & \psi = 0, \quad \omega = -\frac{\partial^2 \psi}{\partial x^2}, \quad \theta = 0, \quad \frac{\partial \phi}{\partial x} = -\frac{Le \cdot Nt \cdot D_T}{C_0 \cdot D_B} \frac{\partial \theta}{\partial x} \quad \text{at } x = 0 \quad \text{and } x = 1; \\ & \psi = 0, \quad \omega = -\frac{\partial^2 \psi}{\partial y^2}, \quad \frac{\partial \theta}{\partial y} = 0, \quad \frac{\partial \phi}{\partial y} = 0 \quad \text{at } y = 0 \quad \text{and } y = 1; \\ & \psi = 0, \quad \omega = -\frac{\partial^2 \psi}{\partial n^2}, \quad \left\{ \begin{aligned} \theta_f &= \theta_{hs}, & \frac{\partial \phi}{\partial n} &= -\frac{Le \cdot Nt \cdot D_T}{C_0 \cdot D_B} \frac{\partial \theta_f}{\partial n} \end{aligned} \right. \quad \text{at the surface heater} \end{aligned} \quad (19)$$

Here, $Ra = g \cdot (\rho\beta)_f \cdot \Delta T \cdot L^3 / [\mu_f(T_c) \cdot \alpha_f]$ is the Rayleigh number, $Le = \alpha_f / \bar{D}_B(T_c)$ is the Lewis number, $Nt = \bar{D}_T(T_c, C_0) \cdot \Delta T / (\alpha_f \cdot T_c)$ is the thermal diffusion coefficient, and auxiliary functions M, K, D_B and D_T have the following form:

The formulated governing equations of nanofluid thermal convection within a closed chamber with a hot element of periodic heat generation with additional restrictions (19) have been worked out using the finite difference methodology on a uniform calculation mesh. The developed mathematical model has been tested using the natural convection

$$M = \left\{ -69.67 + \frac{1593.7}{\theta \Delta T + T_c - 273.15} + 123.8 \cdot \phi C_0 + \frac{135614.0}{[\theta \Delta T + T_c - 273.15]^2} - 25.9 \cdot (\phi C_0)^2 - \frac{3088.0 \cdot \phi C_0}{\theta \Delta T + T_c - 273.15} - \frac{1965274.0}{[\theta \Delta T + T_c - 273.15]^3} + 1.593 \cdot (\phi C_0)^3 + \frac{438.206 \cdot (\phi C_0)^2}{\theta \Delta T + T_c - 273.15} + \frac{14757.3 \cdot \phi C_0}{[\theta \Delta T + T_c - 273.15]^2} \right\} / \left(2.414 \cdot 10^{\frac{247.8}{T_c - 140}} \right)$$

$$K = 1 + 64.7(\phi C_0)^{0.764} \left(\frac{d_f}{d_p} \right)^{0.369} \left(\frac{k_f}{k_p} \right)^{0.7476} \left(\frac{2.414 \times 10^{-5} \times 10^{\frac{247.8}{\theta \Delta T + T_c - 140}}}{\rho_f \alpha_f} \right)^{0.9955} \times \left\{ \frac{\rho_f k_B}{3\pi l_f} \frac{\theta \Delta T + T_c}{5.8274 \times 10^{-10} \cdot 10^{\frac{495.6}{\theta \Delta T + T_c - 140}}} \right\}^{1.2321}$$

$$D_B = \frac{T \cdot \mu_f(T_c)}{T_c \cdot \mu_f(T)} = 10^{\frac{247.8 \cdot \theta \Delta T}{(T_c - 140)(\theta \Delta T + T_c - 140)}} \left[\theta \frac{\Delta T}{T_c} + 1 \right]$$

Table 2 Comparison of mean Nu with results of Ho et al. [45] and Saghir et al. [46]

	ϕ	The presented results	Ho et al. [45]	Saghir et al. [46]
$Ra = 8.663 \times 10^7$	0.01	31.6043	32.2037	30.657
$Pr = 7.002$	0.02	31.2538	31.0905	30.503
	0.03	30.829	29.0769	30.205

problems inside isothermally heated cavities (see Ho et al. [45] and Saghir et al. [46]). Table 2 demonstrates a comparison of the obtained results with the data of other researchers. It can be found that the received data have a good agreement with experimental and numerical outcomes.

The developed solution method has been tested for sensitivity to grid parameters for $Ra = 10^6$, $Pr = 6.52$, $Le = 9415.6$, $C_0 = 0.04$, $\gamma = 0.01$, $Nt = 2.56^{-7}$, $\delta = 0.4$ (see Fig. 2). The results obtained show a periodic change in the average temperature due to periodic heat generation from the local source. Time moments around $\tau = 150$ and $\tau = 314$ characterize the peaks of heat generation oscillations from the heater according to the selected ratio. The use of different grid dimensions for the maximum heat flux leads to small differences between the values of the average heater temperature due to the uniform grid type. It should be noted that these differences decrease when the grid is crunched. Taking into account this grid convergence and computational time, the uniform mesh of 100×100 elements has been employed for further calculations.

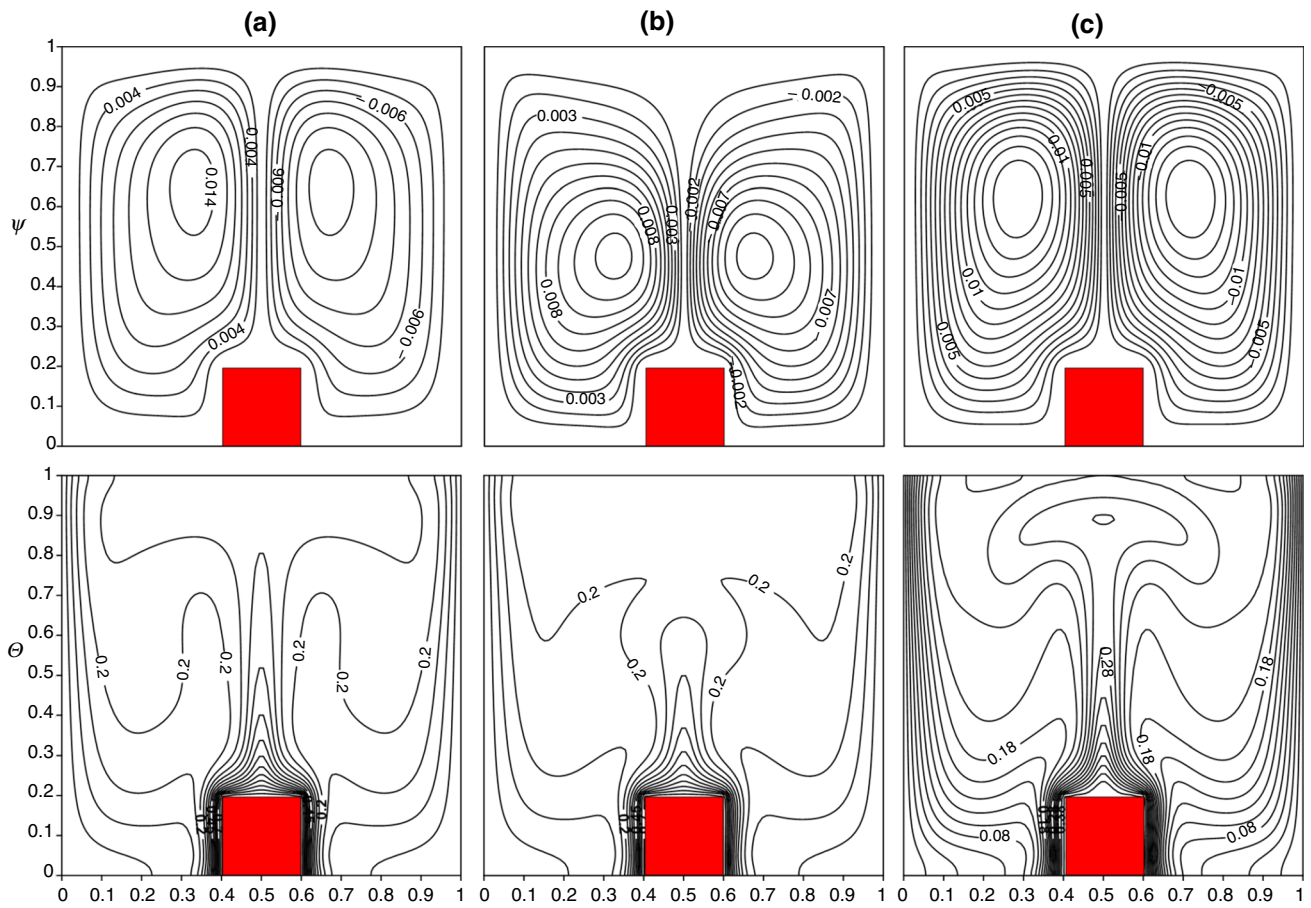


Fig. 3 Isotherms Θ and streamlines Ψ for $C_0=0.04$: $a-\gamma=0.01$, $b-\gamma=0.05$, $c-\gamma=0.1$

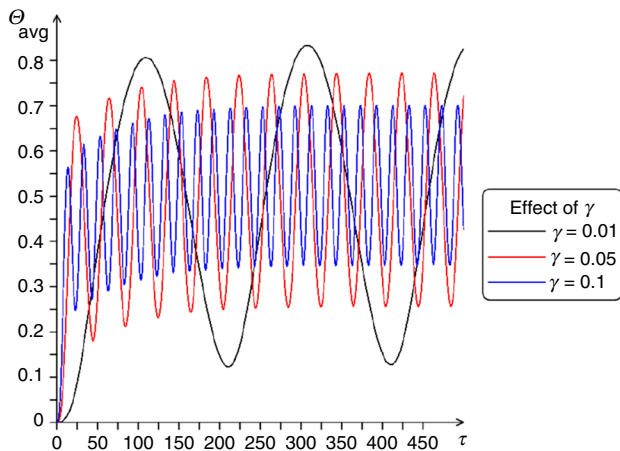


Fig. 4 Time variations of the mean heater temperature at $C_0=0.04$ and different values of γ

Results and discussions

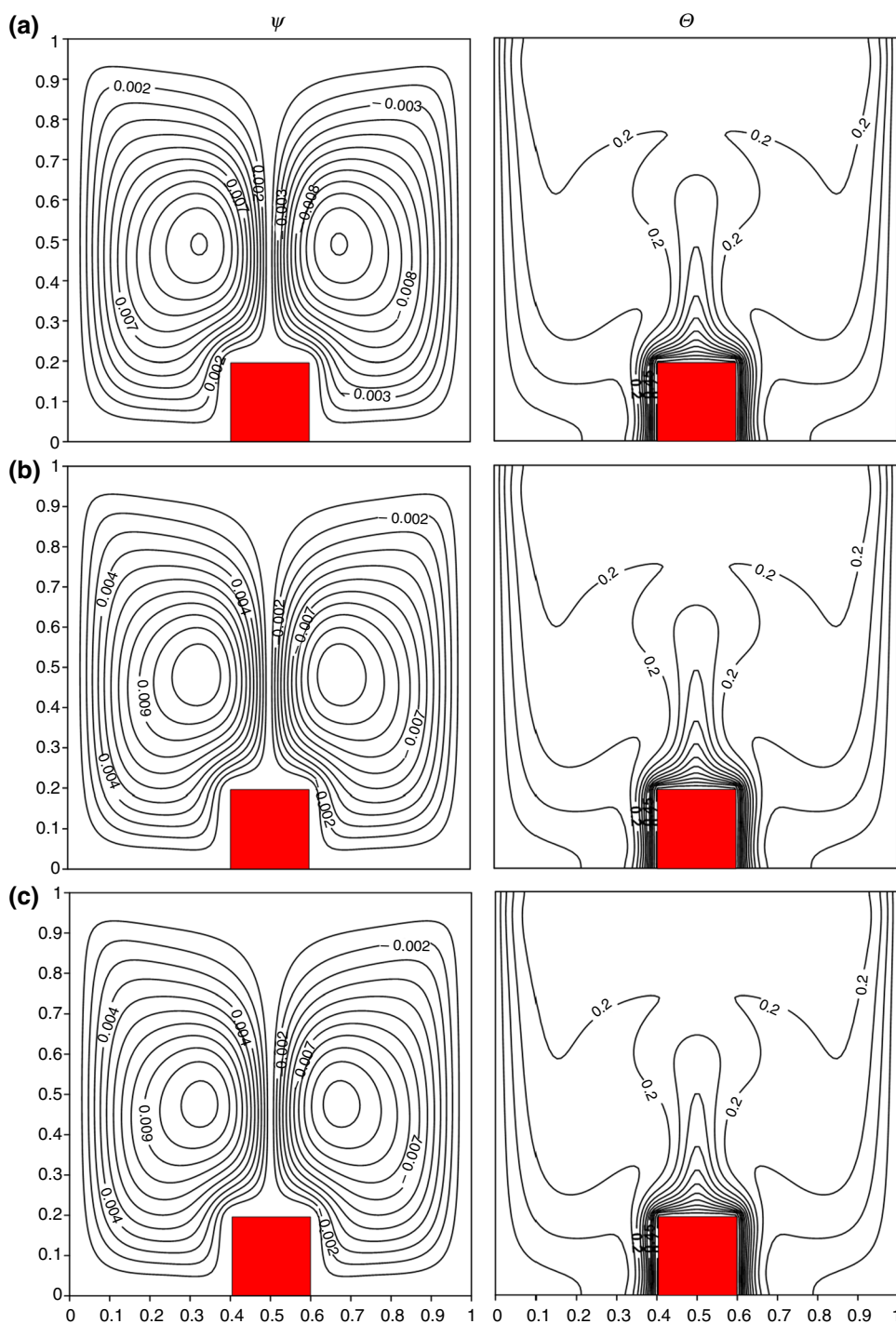
Computational studies of the problem have been solved for $Ra = 10^6$, $Pr = 6.52$, $Le = 9415.6$, $Nt = 2.56^{-7}$,

$C_0 = 0.00 - 0.04$, $\gamma = 0.01 - 0.1$, $\delta = 0.1 - 0.7$, $\tau = 0 - 500$. The major attention was employed to the influence of these dimensionless parameters on thermogravitational energy transport within a closed area saturated with nanosuspension in the presence of a heating element with periodic generation.

Figure 3 reflects the influence of the volumetric thermal production oscillation frequency γ on the distribution of the streamlines and isothermal for other fixed parameters: $C_0 = 0.04$ and $\tau = 500$. Uniform heating of the cavity is observed for any value of γ . The isolines are distributed symmetrically about the average section along the x -coordinate through the heater. Two convective symmetrical cells are formed with cores in the region above the source, which reflects an appearance of ascending and descending convective flows in the chamber due to the cooling effect from the vertical walls.

An increase in the volumetric thermal production oscillation frequency γ enhances the energy transport in the chamber. The convective cores will mix closer to the upper boundary of the cavity. In addition, a decrease in the values of isotherms is observed. The convective plume above

Fig. 5 Isotherms Θ and streamlines Ψ at $\gamma=0.05$, $\delta=0.04$:
 $a - C_0=0.00$, $b - C_0=0.02$,
 $c - C_0=0.04$



the heater narrows at the base and expands near the upper adiabatic wall, reflecting an increase in heat removal from the source. Thus, increasing the intensity of heat generation from the heater leads to increased movement of the suspension in the cavity and mixing of nanoparticles with the base liquid, which leads to improved heat removal.

In more detail, the influence of γ on heat and mass transfer can be estimated from the change in the average

temperature of the heater, which is shown in Fig. 4. As noted above, the distribution of Θ_{avg} has a periodic nature of change. An increase in γ results to a reduction in the period and amplitude of oscillations. It should be noted that the maximum temperature is observed at the minimum value of the considered parameter, while the minimum value is reached at the maximum γ . The transition from a heat

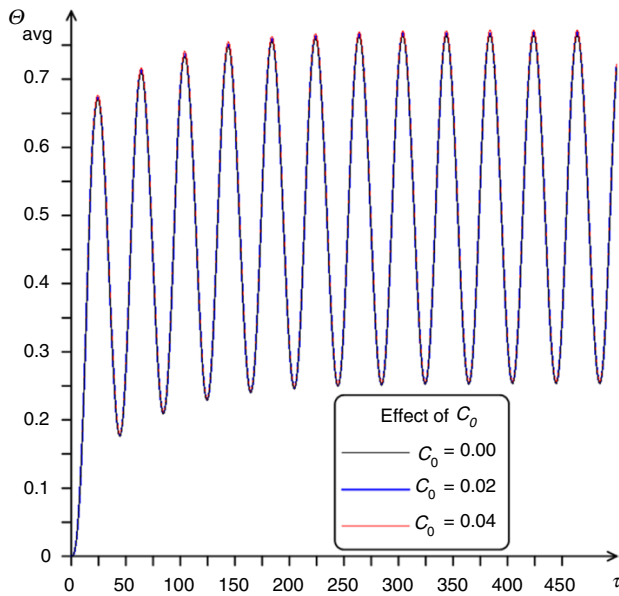


Fig. 6 Change in the average temperature of the heater at $\gamma=0.05$ and different C_0

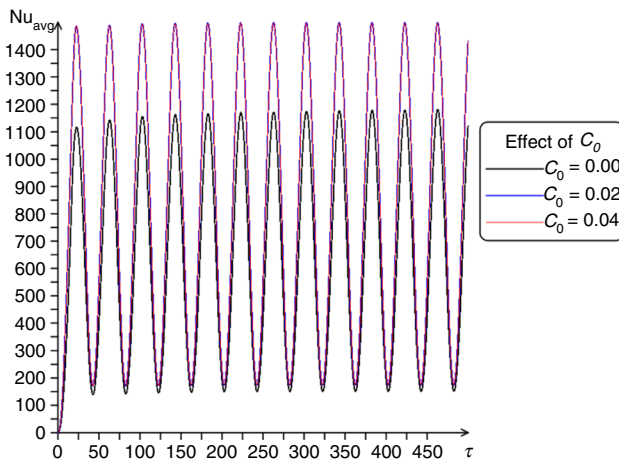


Fig. 7 Time variations of the mean Nu at $\gamma=0.05$ and different C_0

dissipation parameter value of 0.01 to 0.1 reduces the average temperature by 20%.

Figure 5 presents the influence of the initial fraction of nanoadditives (C_0) on the convective energy transport in the considered chamber for fixed dimensionless parameters: $\gamma=0.05$ and $\tau=500$. The change in C_0 has insignificant effect on the streamlines and isotherms. When passing from $C_0=0.00$ to $C_0=0.04$, there is a slight shift of the streamlines Ψ and isotherms Θ to the heater. It can be explained by

the steady state of the process for the considered time point, at which the fluid flow calms down, and the displacement of the base fluid with nanoparticles is established. At the same time, the dependences of the average source temperature did not change (see Fig. 6).

Figure 7 shows the influence of C_0 on the mean Nu along the energy source at $\gamma=0.05$. The results show a strong change in the values of the Nusselt number when going from $C_0=0.0$ to $C_0=0.02$. Further increase in C_0 has no noticeable effect on Nu_{avg} . Thus, the addition of nanoparticles CuO into the base liquid leads to an increase in the intensification of heat transfer at the source surface by 25%, which indicates the intensification of heat exchange.

Numerical calculations of thermogravitational convection in a chamber has been performed for various positions of the heat-producing solid block ($\delta=//L$). The obtained distributions of isotherms and streamlines for various δ and for $C_0=0.04$, $\gamma=0.05$ are shown in Fig. 8. The distribution of streamlines demonstrates a symmetrical flow structure respect to the hot element location. It should be noted that for $\delta=0.1, 0.7$, one huge convective cell appears with a core in the central part of the cavity. When the source is displaced to the right isothermal boundary, the convective cells are aligned, and at $\delta=0.4$ (see Fig. 8d), a completely symmetrical flow with respect to the central section is observed. A further raise of δ results to a repetition of the initial flow pattern in the reflected form. Moving the source to different parts of the cavity away from the center enhances the cooling effect of the vertical walls with increasing boundary layers between the source and the boundaries.

The distributions of the integral characteristics of energy transport at different locations of the heater (average temperature source is in Fig. 9 and the mean Nu at the source is in Fig. 10) reflect a weak influence of δ . In any case, results illustrate a periodic change in the considered parameters due to the oscillation of the volumetric heat generation of the heater. For clarity, the time moment up to $\tau=200$ has been considered and the central position of the source relative to the middle section ($\delta=0.4$) as well as the symmetrical locations of the relative central section ($\delta=0.1$ and $\delta=0.7$, $\delta=0.3$ and $\delta=0.5$) have been considered. The minimum temperature in this case is observed at the central location of the heater ($\delta=0.4$), while the displacement of the source increases the temperature, and the temperature values for symmetrical locations coincide: $\delta=0.1$ and $\delta=0.7$, $\delta=0.3$ and $\delta=0.5$.

In addition, the time dependences of the mean Nusselt number (Fig. 10) reflects nonsignificant differences for various values of δ due to the conservation of the heat flux and

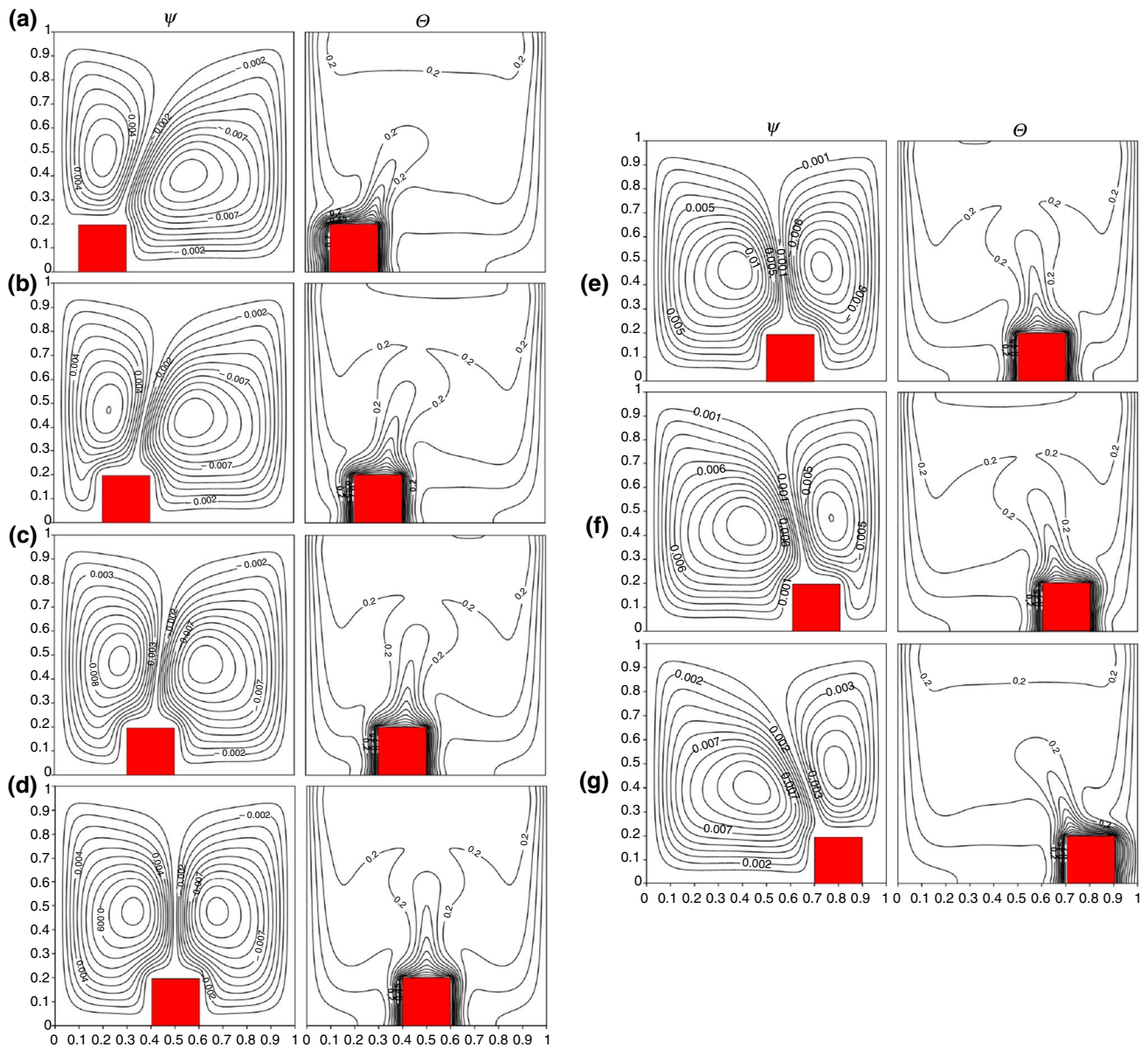


Fig. 8 Effect of the position of the hot element on isotherms Θ and isolines of Ψ at $C_0=0.04$, $\gamma=0.05$ for different hot element location δ : $a-\delta=0.1$, $b-\delta=0.2$, $c-\delta=0.3$, $d-\delta=0.4$, $e-\delta=0.5$, $f-\delta=0.6$, $g-\delta=0.7$

by compensating for the effect of cooling walls with a symmetric arrangement.

Figure 11 shows the dynamics of flow development in the cavity using the example of isotherms Θ and isolines of the stream function Ψ during one oscillation period. For this, the case of $C_0=0.02$, $\gamma=0.05$ and the last considered oscillation period for $\tau=445-485$ have been considered. The following time points have been used: $\tau=445$ (Fig. 11a), $\tau=455$ (Fig. 11b), $\tau=465$ (Fig. 11c), $\tau=475$ (Fig. 11d), and

$\tau=485$ (Fig. 11e). The resulting distributions clearly reflect the evolution of convective flows in the cavity during the oscillation period. It should be noted that the intensification of heat and mass transfer is achieved at $\tau=T_\tau/2$ (Fig. 11c), where T_τ is the oscillation period. The presence of CuO solid particles in the base fluid improves the thermal conductivity properties of the suspension and improves the properties of the passive cooling system.

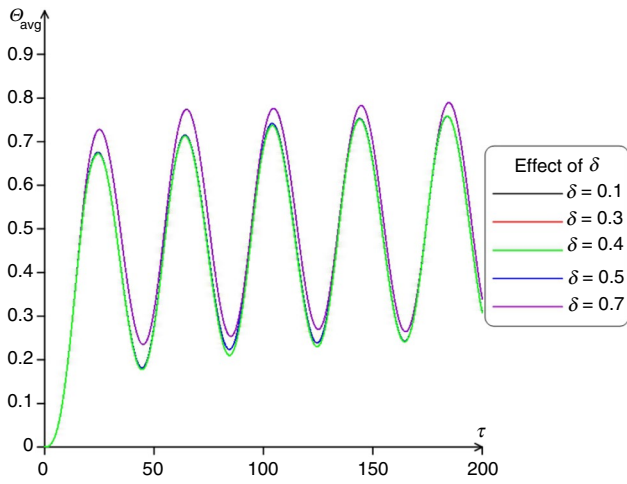


Fig. 9 Time variations of the mean heater temperature at $\gamma=0.05$, $C_0=0.04$ and different δ

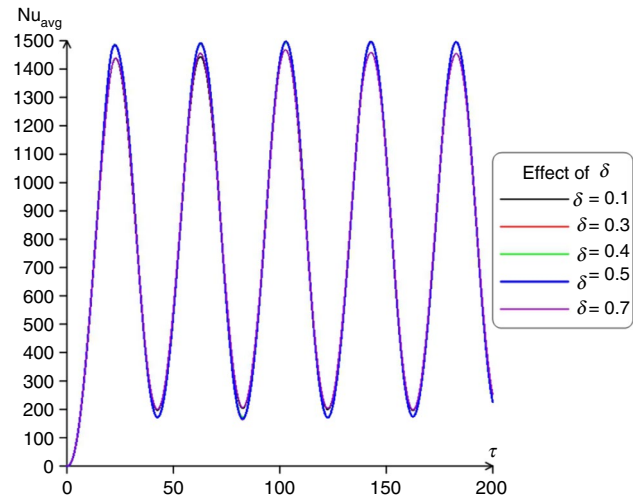


Fig. 10 Time variations of the mean Nu at $\gamma=0.05$, $C_0=0.04$ and different δ

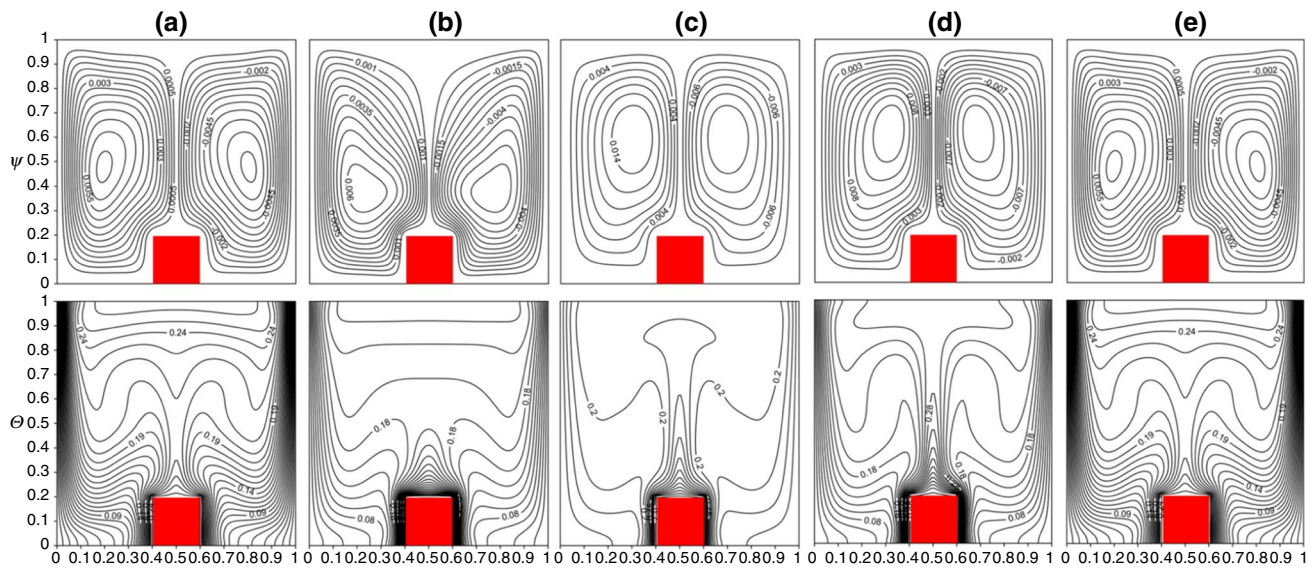


Fig. 11 Isotherms Θ and isolines of Ψ at $C_0=0.02$, $\gamma=0.05$ for different moments of one period of oscillation: $a-\tau=445$, $b-\tau=455$, $c-\tau=465$, $d-\tau=475$, $e-\tau=485$

Conclusions

A numerical investigation of the phenomenon of convective energy and mass transport in a closed square chamber saturated with H_2O/CuO nanosuspension under the impact of an energy source of periodic heat generation has been carried out. The cavity has been cooled from the vertical walls of a constant low temperature. The control equations have been written using the dimensionless stream function, vorticity, temperature and solved by the finite difference method using a developed C++ programming code. As a result of the present research the following conclusions have been obtained:

- The introduction of copper nanoparticles results to an increase in energy transport rate in the cavity compared to a pure working liquid.
- The periodic law of source heating leads to a periodic change in the integral characteristics of heat transfer such as Θ_{avg} and Nu_{avg} . In this case, the intensity of heat generation is reflected in the change in the periods and amplitudes of the distributions.
- Changing the location of the heater does not lead to qualitative changes in the characteristics of heat transfer.
- An addition of nanoparticles into the water-based fluid and varying the properties of the working fluid and heat transport can improve the heat transfer by 20–25%.

The analyzed problem and obtained results can be considered as the further development of one of the main directions of hydrodynamics and thermophysics, namely the optimization of thermal systems with heating elements of complex types (for the present research using the periodic inner heating). Therefore, the novelty of the present research is related to analysis of cooling schemes for solid element of periodic volumetric heat generation using nanofluids of variable physical properties. Such analysis is performed for the first time taking into account the published papers. In addition, the conclusions about the influence of the heater position on the heat transfer rate and nanofluid convective flows strength within the cavity are new.

Acknowledgements This study was supported by the Tomsk State University Development Programme (Priority–2030). The authors would like to thank very much to the very competent Reviewers for their valuable time spent on reading the manuscript and for the valuable comments and suggestions.

References

- Choi SUS. Enhancing thermal conductivity of fluids with nanoparticles. In: Proceedings of the 1995 ASME international mechanical engineering congress and exposition, FED 231/MD 66; 1995. p. 99–105.
- Das SK, Choi SUS, Yu W, Pradeep Y. Nanofluids: science and technology. New Jersey: Wiley; 2008.
- Nield DA, Bejan A. Convection in porous media. 5th ed. New York: Springer; 2017.
- Shenoy A, Sheremet M, Pop I. Convective flow and heat transfer from wavy surfaces: viscous fluids, porous media and nanofluids. New York: CRC Press, Taylor & Francis Group; 2016.
- Merkin JH, Pop I, Lok YY, Groşan T. Similarity solutions for the boundary layer flow and heat transfer of viscous fluids, nanofluids, porous media, and micropolar fluids. Oxford: Elsevier; 2021.
- Miroshnichenko IV, Sheremet MA, Oztop HF, Abu-Hamdeh N. Natural convection of $\text{Al}_2\text{O}_3/\text{H}_2\text{O}$ nanofluid in an open inclined cavity with a heat-generating element. *Int J Heat Mass Transf.* 2018;126:184–91.
- Bouchoucha AEM, Bessaïh R, Oztop HF, Al-Salem K, Bayrak F. Natural convection and entropy generation in a nanofluid filled cavity with thick bottom wall: effects of non-isothermal heating. *Int J Mech Sci.* 2017;126:95–105.
- Bondarenko DS, Sheremet MA, Oztop HF, Ali ME. Natural convection of $\text{Al}_2\text{O}_3/\text{H}_2\text{O}$ nanofluid in a cavity with a heat-generating element. Heatline visualization. *Int J Heat Mass Transf.* 2019;130:564–74.
- Mahmoodi M. Numerical simulation of free convection of nanofluid in a square cavity with an inside heater. *Int J Therm Sci.* 2011;50:2161–75.
- Keramat F, Dehghan P, Mofarahi M, Lee C. Numerical analysis of natural convection of alumina-water nanofluid in H-shaped enclosure with a V-shaped baffle. *J Taiwan Inst Chem Eng.* 2020;111:63–72.
- Islam Z, Azad AK, Hasan MdJ, Hossain R, Rahman MM. Unsteady periodic natural convection in a triangular enclosure heated sinusoidally from the bottom using CNT-water nanofluid. *Results Eng.* 2022;14:100376.
- Nabwey HA, Rashad AM, Khan WA, Alshber SI. Effectiveness of magnetize flow on nanofluid via unsteady natural convection inside an inclined U-shaped cavity with discrete heating. *Alex Eng J.* 2022;61:8653–66.
- Alsabery AI, Vaezi M, Tayebi T, Hashim I, Ghalambaz M, Chamkha AJ. Nanofluid mixed convection inside wavy cavity with heat source: a non-homogeneous study. *Case Stud Therm Eng.* 2022;34:102049.
- Narankhishig Z, Ham J, Lee H, Cho H. Convective heat transfer characteristics of nanofluids including the magnetic effect on heat transfer enhancement—a review. *Appl Therm Eng.* 2021;193:116987.
- Sheikholeslami M, Rokni HB. Simulation of nanofluid heat transfer in presence of magnetic field: a review. *Int J Heat Mass Transf.* 2017;115:1203–33.
- Selimefendigil F, Ismael MA, Chamkha AJ. Mixed convection in superposed nanofluid and porous layers in square enclosure with inner rotating cylinder. *Int J Mech Sci.* 2017;124–125:95–108.
- Vijaybabu TR. Influence of permeable circular body and $\text{CuO}/\text{H}_2\text{O}$ nanofluid on buoyancy-driven flow and entropy generation. *Int J Mech Sci.* 2020;166:105240.
- Biswas N, Manna NK, Datta P, Mahapatra PS. Analysis of heat transfer and pumping power for bottom-heated porous cavity saturated with Cu-water nanofluid. *Powder Technol.* 2018;326:356–69.
- Sivasankaran S, Alsabery AI, Hashim I. Internal heat generation effect on transient natural convection in a nanofluid-saturated local thermal non-equilibrium porous inclined cavity. *Phys A.* 2018;509:275–93.
- Garoozi F, Hoseininejad F, Rashidi MM. Numerical study of natural convection heat transfer in a heat exchanger filled with nanofluids. *Energy.* 2016;109:664–78.
- Emami RY, Siavashi M, Moghaddam GS. The effect of inclination angle and hot wall configuration on Cu-water nanofluid natural convection inside a porous square cavity. *Adv Powder Technol.* 2018;29:519–36.
- Bouzerzour A, Djeddar M, Oztop HF, Tayebi T, Abu-Hamdeh N. Natural convection in nanofluid filled and partially heated annulus: effect of different arrangements of heaters. *Phys A.* 2020;538:122479.
- Du R, Gokulavani P, Muthamilselvan M, Al-Amri F, Abdalla B. Influence of the Lorentz force on the ventilation cavity having a centrally placed heated baffle filled with the $\text{Cu}-\text{Al}_2\text{O}_3-\text{H}_2\text{O}$ hybrid nanofluid. *Int Commun Heat Mass Transfer.* 2020;116:104676.
- Nath R, Murugesan K. Double diffusive mixed convection in a $\text{Cu}-\text{Al}_2\text{O}_3/\text{water}$ nanofluid filled backward facing step channel with inclined magnetic field and part heating load conditions. *J Energy Storage.* 2022;47:103664.
- Rana P, Kumar A, Gupta G. Impact of different arrangements of heated elliptical body, fins and differential heater in MHD convective transport phenomena of inclined cavity utilizing hybrid nanofluid: artificial neural network prediction. *Int Commun Heat Mass Transf.* 2022;132:105900.
- Roy NC. Flow and heat transfer characteristics of a nanofluid between a square enclosure and a wavy wall obstacle. *Phys Fluids.* 2019;31:082005.
- Roy NC. Natural convection in the annulus bounded by two wavy wall cylinders having a chemically reacting fluid. *Int J Heat Mass Transf.* 2019;138:1082–95.
- Roy NC. Modeling of a reactor with exothermic reaction bounded by two concentric cylinders. *Phys Fluids.* 2018;30:083604.
- Roy NC. MHD natural convection of a hybrid nanofluid in an enclosure with multiple heat sources. *Alex Eng J.* 2022;61:1679–94.

30. Roy NC, Hossain MdA, Gorla RSR, Siddiqua S. Natural convection around a locally heated circular cylinder placed in a rectangular enclosure. *J Non-Equilib Thermodyn.* 2021;46(1):45–59.
31. Parvin S, Roy NC, Saha LK, Siddiqua S. Heat transfer characteristics of nanofluids from a sinusoidal corrugated cylinder placed in a square cavity. *Proc Inst Mech Eng Part C J Mech Eng Sci.* 2022;236(5):2617–30.
32. Saha L, Saha LK, Bala S, Roy NC. Natural convection flow in a fluid-saturated non-Darcy porous medium within a complex wavy wall reactor. *J Therm Anal Calorim.* 2020;146:325–40.
33. Sajid HU, Ali HM. Recent advances in application of nanofluids in heat transfer devices: a critical review. *Renew Sustain Energy Rev.* 2019;103:556–92.
34. Sajid MU, Bicer Y. Nanofluids as solar spectrum splitters: a critical review. *Sol Energy.* 2020;207:974–1001.
35. Sajid MU, Bicer Y. Performance assessment of spectrum selective nanofluid-based cooling for a self-sustaining greenhouse. *Energy Technol.* 2021;9:2000875.
36. Sajid HU, Ali HM, Yusuf B. Energetic performance assessment of magnesium oxide-water nanofluid in corrugated omnichannel heat sinks: an experimental study. *Int J Energy Res.* 2020. <https://doi.org/10.1002/er.6024>.
37. Sajid MU, Ali HM, Sufyan A, Rashid D, Zahid SU, Rehman WU. Experimental investigation of TiO₂-water nanofluid flow and heat transfer inside wavy mini-channel heat sinks. *J Therm Anal Calorim.* 2019;137:1279–94.
38. Hawaz S, Ali HM, Sajid MU, Said Z, Tiwari AK, Sundar LS, Li C. Oriented square shaped pin-fin heat sink: performance evaluation employing mixture based on ethylene glycol/water graphene oxide nanofluid. *Appl Therm Eng.* 2022;206:118085.
39. Astanina MS, Riahi MK, Abu-Nada E, Sheremet MA. Magneto-hydrodynamic in partially heated square cavity with variable properties: discrepancy in experimental and theoretical conductivity correlations. *Int J Heat Mass Transf.* 2018;116:532–48.
40. Astanina MS, Abu-Nada E, Sheremet MA. Combined effects of thermophoresis, Brownian motion and nanofluid variable properties on CuO-water nanofluid natural convection in a partially heated square cavity. *J Heat Transf.* 2018;140(8):082401.
41. Chon CH, Kihm KD, Lee SP, Choi SUS. Empirical correlation finding the role of temperature and particle size for nanofluid (Al₂O₃) thermal conductivity enhancement. *Appl Phys Lett.* 2005;87:153107.
42. Abu-Nada E, Masoud Z, Oztop HF, Campo A. Effect of nanofluid variable properties on natural convection in enclosures. *Int J Therm Sci.* 2010;49:479–91.
43. Haddad Z, Abu-Nada E, Oztop HF, Mataoui A. Natural convection in nanofluids: are the thermophoresis and Brownian motion effects significant in nanofluid heat transfer enhancement. *Int J Therm Sci.* 2012;57:152–62.
44. Nguyen T, Desgranges F, Roy G, Galanis N, Mare T, Boucher S, Angue Minsta H. Temperature and particle-size dependent viscosity data for water based nanofluids-hysteresis phenomenon. *Int J Heat Fluid Flow.* 2007;28:1492–506.
45. Ho CJ, Liu WK, Chang YS, Lin CC. Natural convection heat transfer of alumina-water nanofluid in vertical square enclosures: an experimental study. *Int J Therm Sci.* 2010;49:1345–53.
46. Saghir MZ, Ahadi A, Mohamad A, Srinivasan S. Water aluminum oxide nanofluid benchmark model. *Int J Therm Sci.* 2016;109:148–58.

Publisher's Note Springer Nature remains neutral with regard to jurisdictional claims in published maps and institutional affiliations.

Springer Nature or its licensor (e.g. a society or other partner) holds exclusive rights to this article under a publishing agreement with the author(s) or other rightsholder(s); author self-archiving of the accepted manuscript version of this article is solely governed by the terms of such publishing agreement and applicable law.